

Journal of Mechanics of Materials and Structures

**CHARACTERIZATION OF CNT PROPERTIES USING
SPACE-FRAME STRUCTURE**

Muhammad Arif and Jacob Muthu

Volume 13, No. 4

July 2018



CHARACTERIZATION OF CNT PROPERTIES USING SPACE-FRAME STRUCTURE

MUHAMMAD ARIF AND JACOB MUTHU

We studied the elastic properties of different carbon nanotubes (CNTs), i.e., pristine and defective single-wall (SWCNTs), double-wall (DWCNTs), and multiwall (MWCNTs) for zigzag and armchair configurations. CNTs atomic geometry was replicated with an equivalent space frame structure (SFS). Coordinates definition of SFS of CNTs was developed in MATLAB code and transferred to the finite element analysis (FEA) software ANSYS. The basic entity of SFS, the C-C chemical bond, was designed as a circular beam with orthotropic properties. The properties were determined by linking the energy equation of molecular mechanics to structural mechanics along with a parametric study. The van der Waals forces between intershells of DWCNTs and MWCNTs were modeled as linear elastic springs in a simplified way. The simplified model avoided the problems due to the nonlinear behavior of van der Waals forces and improved the performance of the FEA software. The effect of chirality, vacancy defects, different diameters, and number of walls on the elastic properties of CNTs were calculated, tabulated, and compared with each other. The result of the proposed SFS model with orthotropic properties was compared with other's results. The space frame structure (SFS) model is found to be better than the equivalent shell model as the defects can be placed at exact locations and a more realistic behavior can be predicted. The SFS models can developed with any type of defect, any number of walls, van der Waals force interactions, and agglomerated forms with variable geometries. These models could be directly embedded in the matrix with a designable interface region to predict tensile and torsional properties of future nanocomposites.

1. Introduction

The discovery of carbon nanotubes (CNTs) [Iijima 1991] has attracted immense interest in the field of high strength structural composite materials due to CNTs extraordinary mechanical properties (elastic modulus 0.5–5 TPa and tensile strength 50–200 GPa) [Qian et al. 2002; Treacy et al. 1996]. These mechanical properties made them as a potential contender for reinforcing matrices such as polymer [Muthu and Dendere 2014], ceramic [Inam et al. 2014], and metal [Tjong 2013]. Mahmoud [Shokrieh et al. 2013] and Kundalwal [Kundalwal and Ray 2014] have shown that adding a small amount of CNTs to the polymer matrix improved the mechanical, thermal, and electrical properties of the composites. Other research works [Inam et al. 2014; Sharma and Shukla 2014] have also reported that the addition of 1% CNTs increased the elastic modulus, flexural, and tensile strength of epoxy composites by 49%, 38%, and 52% respectively.

However, these experimental results are much lower than the theoretically expected values for CNT reinforced composites [Zuberi and Esat 2015]. Researchers have attributed these discrepancies between

Keywords: carbon nanotubes, numerical modeling, continuum Mechanics, finite element analysis, properties.

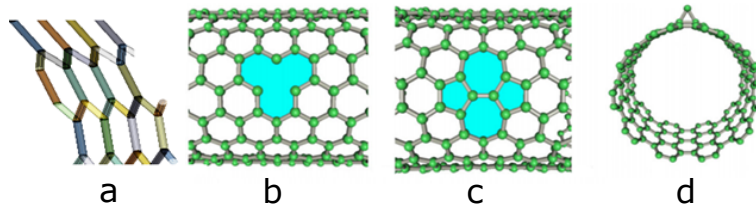


Figure 1. Different kinds of defects in CNTs: hexagonal arrangement (a), vacancy defect (b), Stone–Wales defect (c), adatom (d).

experimental and theoretical results to the inconsistency in CNT diameter [Nam et al. 2015], chirality (rolled up angle of graphene sheet) [Ranjbartoreh and Wang 2010], number of CNT walls [Jia et al. 2011], and defects in the CNT structure [Xiao and Hou 2006]. Different kinds of defects such as vacancy, Stone–Wales, and adatom (Figure 1) are developed in CNTs during synthesis [Tachibana 2013] and play an important role in defining their properties. Researches [Yang et al. 2016] have shown that the vacancy defects (Figure 1b) are the most influential factor in degrading the overall CNT properties. In addition, as pointed out by Popov et al. [Popov et al. 2000] that the properties of CNTs along the tube axial direction are always greater than the transverse directions (orthotropic behavior) and a similar conclusion was also drawn by Kundalwal and Kumar [Kundalwal and Kumar 2016]. Therefore, it is essential to understand the effect of the above factors (diameter, chirality, number of walls, vacancy defects, and the orthotropic behavior) on the CNTs mechanical properties, which will further be helpful in choosing suitable CNTs as composites reinforcement to obtain improved mechanical properties.

Various experimental techniques such as Raman spectroscopy, scanning electron spectroscopy, transmission electron microscopy, nanoindentation, and x-ray diffraction have been used to characterize the CNT's properties [Chabalala et al. 2011]. However, the main challenges faced with these experimental techniques are that they are either expensive or technically not feasible to obtain the nanoscale behavior of CNTs. Moreover, the conventional theoretical models such as rule of mixtures [Han et al. 2014b], effective field models [Zohdi and Wriggers 2005], and continuum mechanics models [Tserpes et al. 2008] also have limitations in predicting the behavior of CNTs at nanolength scales [Han et al. 2014b]. Hence, researchers have focused on developing molecular scale models such as molecular dynamics (MD) and molecular mechanics (MM) methods. These methods are powerful and can provide details at the molecular scale level. However, their limitations in analyzing the number of atoms, length, and time scales along with the computational cost have restricted their applications within a limited span [Han et al. 2014a].

To overcome the length scale limitations in molecular models, an equivalent continuum model (ECM) was proposed [Hernández-Pérez and Avilés 2010]. In the ECM model, the individual carbon nanotube was modeled either as a shell or as a beam with isotropic properties [Roy Chowdury et al. 2014; Hu et al. 2007]. Moreover, in these models, the hexagonal atomic structure of a CNT was completely ignored [Muc 2011] and thus resulted in exaggerated CNT properties. In addition, these models could not include the effects of vacancy defects, chirality, and van der Waals force interactions between the walls. Hence, for incorporating the CNTs atomic structure, a space frame structure (SFS) model was proposed [Ghavamian et al. 2013]. In the SFS model, the chemical bond between two carbon atoms (C-C) was modeled as a circular beam with isotropic properties in such a way that one carbon molecule was modeled using six

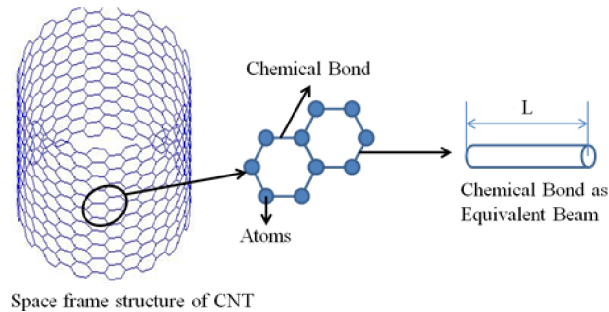


Figure 2. Equivalent SFS.

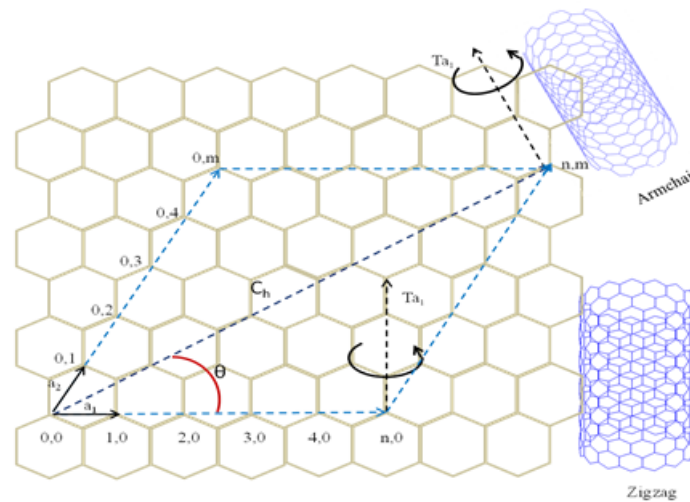


Figure 3. Rolling angle and chiral vector.

circular beams in a hexagonal shape, as shown in Figure 2. The chemical bond properties were obtained from both solid and molecular mechanic analysis.

However, the CNTs orthotropic properties [Muc 2010] were again ignored by the SFS model including the other important parameters as explained above. Hence the objectives of this paper were defined as to characterize the zigzag and armchair CNTs using SFS model by considering the effects of CNTs diameters, chirality, number of walls, vacancy defects, and the van der Waals interactions between the walls (double and multiwalled). In addition, this research also focused on understanding the effect of orthotropic behavior of CNTs on their properties.

2. Methodology for simulation

2A. SFS modeling of CNTs. Since CNTs are formed by rolling the graphene sheets, the parameters such as chiral angle (θ) and chiral vector (C_h) define the types of CNTs such as zigzag and armchair. Figure 3 shows a schematic of chiral vector, chiral angle, and the relevant geometrical parameters.

zigzag			armchair		
n	m	diameter (Å)	n	m	diameter (Å)
7	0	5, 481	4	4	5, 424
11	0	8, 61	6	6	8, 13
14	0	10, 96	8	8	10, 84
20	0	15, 657	11	11	14, 916
28	0	21, 92	16	16	21, 696

Table 1. Configuration properties. Note that all MWCNTs have three walls. Furthermore, the intershell distance d_{s-s} range is 3.4 Å–3.8 Å, and the bond length L range is 1.41 Å–1.42 Å [Harik 2011].

The chiral vector (C_h) is mathematically defined by the unit vectors a_1 and a_2 combined with the step integer n and m , which basically determine the chirality or twist of the nanotube:

$$\vec{C}_h = n\vec{a}_1 + m\vec{a}_2. \quad (2-1)$$

Different roll-up directions of graphene (chiral angle, θ) give different configurations of CNTs and are defined by

$$\theta = \sin^{-1} \left[\frac{\sqrt{3}m}{2(n^2 + nm + m^2)} \right], \quad (2-2)$$

where θ is the chiral angle.

Mathematically, if the step integers $n \neq 0$ and $m = 0$ ($\theta = 0^\circ$) are set then a zigzag CNT could be defined and an armchair structure could be generated for the step integers $n = m$ ($\theta = 30^\circ$) [Rahmandoust and Öchsner 2009]. In addition, the CNTs diameters are also obtained using the step integers as

$$d = 0.783\sqrt{n^2 + nm + m^2} \quad (2-3)$$

2B. CNTs model development. Using the above equations, a CNT was modeled by defining its coordinates in a MATLAB code for the different types of CNTs such as zigzag, armchair, single, defective, double, and multiwall. The required chiral angle and chiral vector were obtained and given in Table 1.

A general methodology that followed for producing both zigzag or armchair configurations was that a basic unit cell (a carbon molecule) was developed along the tube circumference. At first, a single carbon molecule was divided into six equivalent triangles. The height h and half of the base b of the individual triangle were used to draw the positions of the individual carbon atoms and then the carbon molecule unit cell. The angle ψ defines the number of carbon molecules along the circumference based on the base length b with respect to the center of the CNT. Figure 4 shows the schematic of the modeling process.

The base unit cell was then extended further to obtain a base ring and then the full carbon nanotube (Figure 5). Double and multiwall CNTs were developed using the same procedure. The distance between the consecutive walls ($d_{(s-s)}$) was kept at 3.4 ~ 3.8 Å [Ghavamian et al. 2013]. Figure 6 shows the double wall and multiwall CNTs modeled using the proposed procedure.

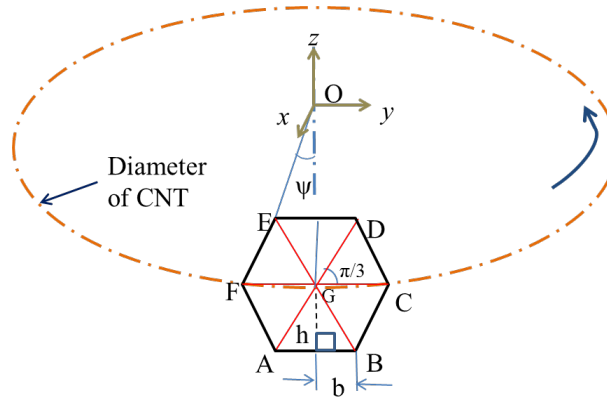


Figure 4. Modeling process of CNTs.

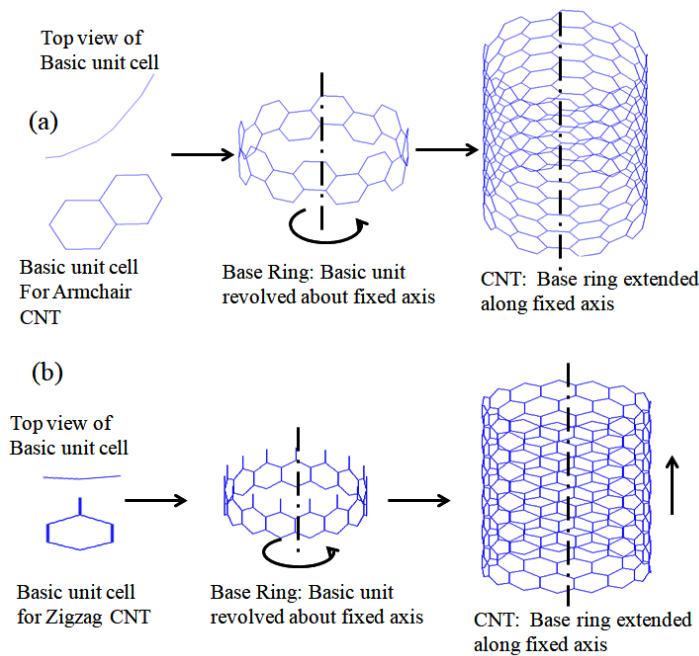


Figure 5. CNTs modeling process: armchair (a) and zigzag (b).

The vacancy defects were randomly generated by removing a point (carbon atom) at three different places: top, center, and bottom of the CNTs. These defects were approximately 120° apart from each other (Figure 7).

The macrofiles containing the CNT coordinates were transferred to ANSYS for developing an IGES-ANSYS workbench multibody CNT model. The in-built ANSYS workbench shared topology method was utilized to convert the multibody CNT SFS-model into a single part. This method joins each equivalent circular beam to the other beams through the edge joints method. Figure 8 shows the transferred ANSYS workbench CNT model developed in MATLAB. Five different diameters were used for both

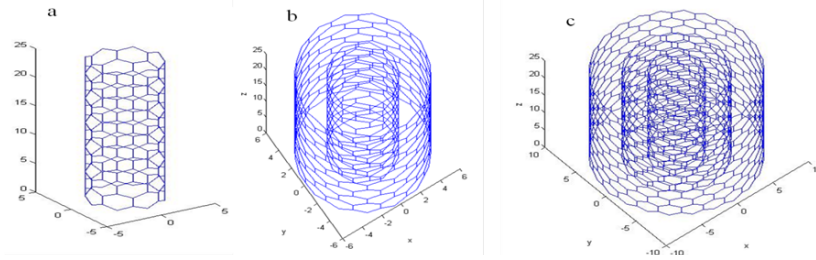


Figure 6. DWCNT and MWCNT modeling process.

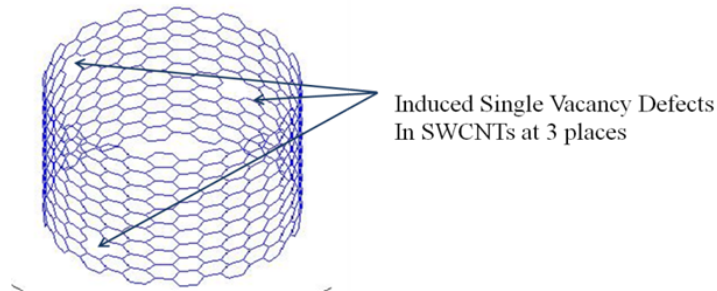


Figure 7. CNT with vacancy defects.

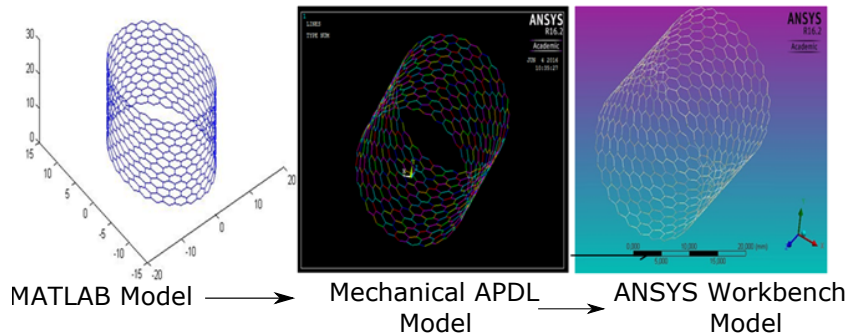


Figure 8. Equivalent SFS modeling process of CNTs.

the zigzag and armchair configurations. Pristine and defective single-walled and pristine double and multiwalled CNTs were considered for the analysis.

2C. C-C chemical bond orthotropic properties. The next step is to define the C-C chemical bond properties. As briefly discussed before, most of the research works have considered CNTs as an isotropic material. However, theoretical studies [Muc 2010] have shown that the CNTs behave like an orthotropic material. Hence, in this research, the orthotropic properties of CNTs were obtained by assuming orthotropic response from the individual C-C bond. Hence two different methods were used to obtain both axial and transverse response of the C-C bonds.

2C1. C-C bond axial direction response. The axial direction response of the C-C bond was obtained by equating the energy of the atomistic system (molecular mechanics) with the beam model (classical

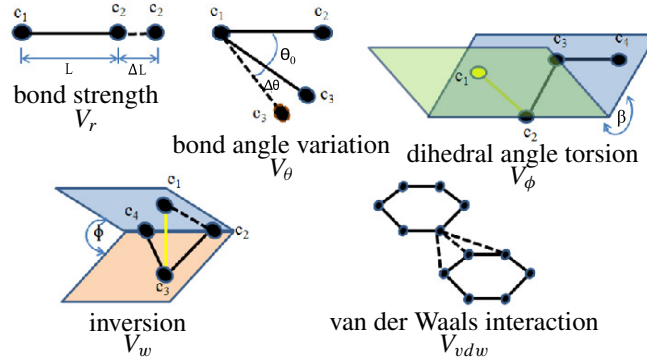


Figure 9. Graphical representation of steric potential energy.

structural mechanics). Based on molecular mechanics, the C-C chemical bond could be expressed using steric potential energies, which gives the total potential energy (V_t) [Rahmandoust and Öchsner 2012] of the individual C-C bond as

$$V_t = \sum V_r + \sum V_\theta + \sum V_\phi + \sum V_w + \sum V_{vdw}, \quad (2-4)$$

where V_r , V_θ , V_ϕ , V_w , V_{vdw} are the bond strength, bond angle variation, dihedral angle torsion, inversion, and interaction strain energies respectively (Figure 9).

Since the inversion and the interaction energies have very little influence on the total potential energy equation, the bond strength, bond angle variation, and dihedral angle torsion energies are only considered for the current analysis. These energies are expressed as

$$V_r = \frac{1}{2}k_r(L - L_0)^2 = \frac{1}{2}k_r(\Delta L)^2, \quad (2-5)$$

$$V_\theta = \frac{1}{2}k_\theta(\theta - \theta_0)^2 = \frac{1}{2}k_\theta(\Delta\theta)^2, \quad (2-6)$$

$$V_\phi = V_w = \frac{1}{2}k_\tau(\Delta\beta)^2. \quad (2-7)$$

Here, k_r , k_θ , and k_τ are bond stretching, bond angle variation, and torsion resistance force constants, respectively; ΔL , $\Delta\theta$, and $\Delta\beta$ are the bond stretching, bond angle variation, and angle variation of bond twist, respectively. The C-C chemical bond characteristics are assumed to be an analogue to a structural mechanics beam element (Figure 10). Here, the carbon atoms act as joints of the beam element and hence the stiffness equations associated with the structural mechanics for a beam element could be equated with the force constants of molecular mechanics to define the C-C chemical bond along the axial direction.

According to classical structural mechanics, the strain energy equations of a beam under uniform axial, bending, and torsional loads are given by

$$U_A = \frac{1}{2} \int_0^L \frac{F^2}{EA} dL = \frac{1}{2} \frac{F^2 L}{EA} = \frac{1}{2} \frac{EA}{L} \Delta L^2, \quad (2-8)$$

$$U_M = \frac{1}{2} \int_0^L \frac{M^2}{EI} dL = \frac{1}{2} \frac{M^2 L}{EI} = \frac{1}{2} \frac{EI}{L} \Delta\theta^2, \quad (2-9)$$

$$U_T = \frac{1}{2} \int_0^L \frac{T^2}{GJ} dL = \frac{1}{2} \frac{T^2 L}{GJ} = \frac{1}{2} \frac{GJ}{L} \Delta\beta^2, \quad (2-10)$$

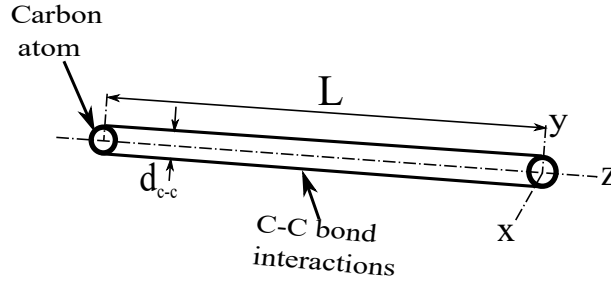


Figure 10. Equivalent beam model.

k_r	$938 \text{ kcal} \cdot \text{mol}^{-1} \cdot \text{Å}^{-2} = 6.52 \times 10^{-7} \text{ N} \cdot \text{nm}^{-1}$
K_θ	$126 \text{ kcal} \cdot \text{mol}^{-1} \cdot \text{Å}^{-2} = 8.76 \times 10^{-10} \text{ N} \cdot \text{nm}^{-1}$
K_τ	$39.986 \text{ kcal} \cdot \text{mol}^{-1} \cdot \text{Å}^{-2} = 2.780 \times 10^{-10} \text{ N} \cdot \text{nm}^{-1}$

Table 2. Molecular mechanics constant values; note that the bond length $L = 0.142 \text{ nm}$ [Tersoff and Ruoff 1994].

where E is the elastic modulus, A is the cross sectional area, L is the beam length, I is the moment of inertia, G is the polar moment of inertia, J is the polar moment of inertia, θ is rotational angle, and β is relative rotation between the two ends.

By considering analogues and equating the corresponding energy equations, the relationship between structural mechanics (EA , EI , and GJ) and the molecular mechanics parameters (k_r , k_θ , and k_τ) are deduced as [Li and Chou 2003b]

$$k_r = \frac{EA}{L}, \quad k_\theta = \frac{EI}{L}, \quad k_\tau = \frac{GJ}{L}. \quad (2-11)$$

These above equations were used to obtain the C-C bond axial direction response. The parameters for calculating the C-C bond axial response are given in Table 2.

Using the above values, the C-C bond axial responses are calculated as

$$d_{c-c} = 4\sqrt{\frac{K_\theta}{K_r}} = 0.14660 \text{ nm}, \quad E_{zz} = \frac{(K_r)^2 L}{4\pi K_\theta} = 5.49 \text{ TPa}, \quad G_{xy} = \frac{(K_r/K_\theta)K_\tau L}{8\pi} = 0.871 \text{ TPa}.$$

2C2. C-C bond transverse direction response. The transverse direction responses of C-C bonds were obtained using an ANSYS parametric study. The space frame structure model of a single-wall zigzag CNT with diameter 0.861 nm was chosen along with the C-C bond axial response values previously obtained for this analysis. The parametric study was carried out by using the range of values of elastic modulus, shear modulus, and Poisson's ratio as given in Table 3. The analysis was repeated until the SFS model radius modulus was equivalent to 650 GPa [Reich et al. 2002]. Then the corresponding orthotropic properties were selected to define the transverse response of the C-C bond interactions.

The overall orthotropic response of the C-C bond is given in Table 4.

elastic modulus (GPa)		shear modulus (GPa)		Poisson's ratio		
E_{xx}	E_{yy}	G_{xy}	G_{yz}	γ_{xy}	γ_{yz}	γ_{xz}
4.5–5.5	4.5–5.5	3–8.71	3–8.71	0.1–0.25	0.1–0.25	0.1–0.25

Table 3. Range of values for parametric study variables.

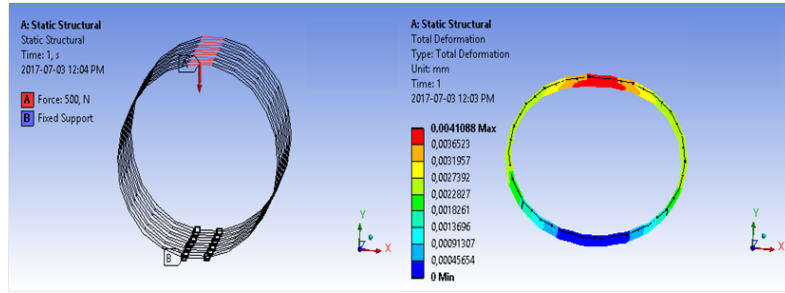


Figure 11. Radial test model.

modulus (GPa)			shear (GPa)		
E_{xx}	E_{yy}	E_{zz}	G_{xy}	G_{yz}	G_{xz}
523	523	5490	409	409	871

Table 4. Orthotropic properties of CNTs. Note that the ratio $\gamma_{xy} = \gamma_{yz} = \gamma_{xz} = 0.1$.

2D. Modeling of van der Waals forces. DWCNTs and MWCNTs contain two or more concentric shells at distances 3.4 Å to 3.8 Å from each other and interact through the van der Waals (F_{vdw}) forces. In addition, these forces are effective within 0.85 nm range [Zuberi and Esat 2015] and the atoms which are not within the range will be coupled with the adjacent range atoms. Based on the above assumption, a single carbon atom of one shell interacts with 58 atoms of an adjacent shell (0.85 nm range) as shown in Figure 12a. Generally, the van der Waals forces are calculated using Lennard–Jones potentials [1924], given as

$$F_{(vdw)} = 4\epsilon \left[-12 \left(\frac{\sigma}{d_{s-s}} \right)^{12} + 6 \left(\frac{\sigma}{d_{s-s}} \right)^6 \right]. \quad (2-12)$$

Ali and coworkers [Ghavamian et al. 2013] modeled the van der Waals force (F_{vdw}) interaction between two carbon atoms as a spring with a stiffness ($K_{\text{single C-C}}$) of 0.24245 N/m. However, with a large number of van der Waals interactions, modeling each interaction could lead to computational difficulties. Hence these intershell interactions were modeled as equivalent springs (Figure 12b).

Four equivalent springs at 90° intervals were inserted between two adjacent shells to model the total van der Waals force interactions. The stiffness of a single equivalent spring (K_{eq}) was calculated from the total spring stiffness K_n . Hence, $K_n = 58 \times K_{\text{single C-C}} \times \text{total number of atomic interactions from first shell to the second shell (TAI)}$.

Where $n = (\text{1st shell, 2nd shell, } \dots)$ and $K_{\text{single C-C}}$ is the spring stiffness between two carbon atoms. The total atomic interactions (TAI) between one shell to the other were estimated by the following

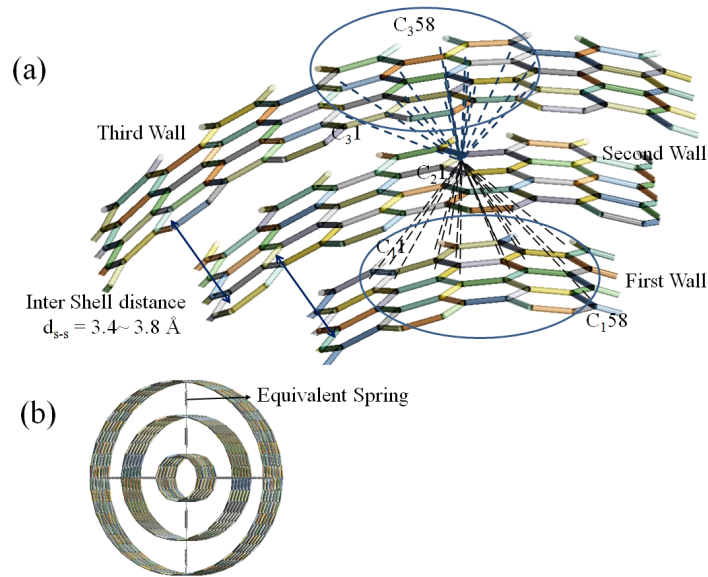


Figure 12. Van der Waals force interactions between different shells (a) and equivalent spring constant between shells (b).

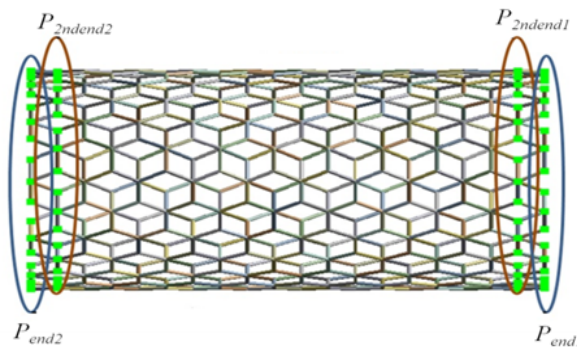


Figure 13. End points of CNTs.

equation:

$$TAI = P_{\text{total}} - 0.5P_{\text{end1}} - 0.5P_{\text{end2}} - 0.875P_{\text{2ndend1}} - 0.875P_{\text{2ndend2}}, \quad (2-13)$$

where P_{total} is the total number of atoms in a single shell, P_{end1} is the number of atoms in the end rows, and P_{2ndend1} is the number of atoms in second end rows (Figure 13).

Since $P_{\text{end1}} = P_{\text{end2}}$ and $P_{\text{2ndend1}} = P_{\text{2ndend2}}$, the TAI equation becomes

$$TAI = P_{\text{total}} - P_{\text{end}} - 1.75P_{\text{2ndend}}.$$

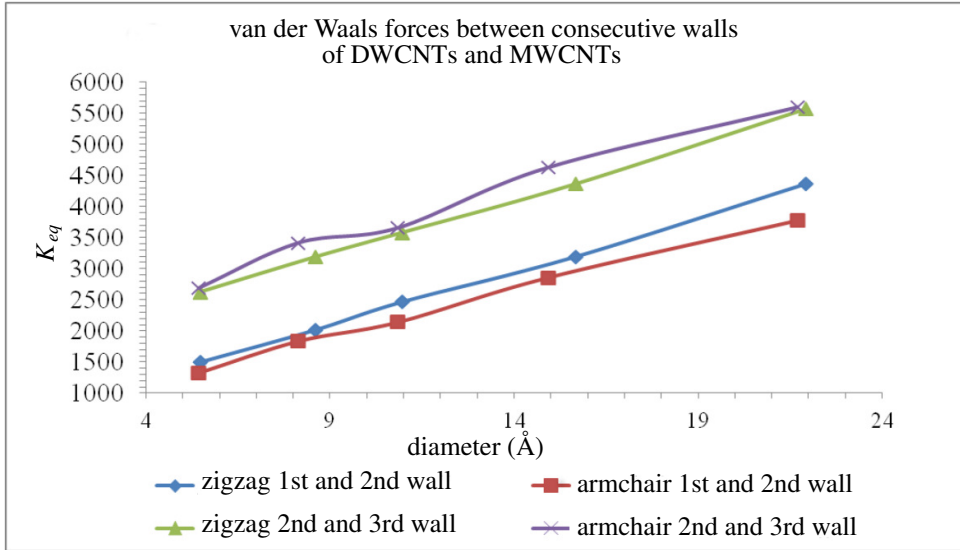


Figure 14. Van der Waals forces between consecutive walls.

Using the above TAI values, the total spring stiffnesses (K_n) were obtained and then K_{eq} for the individual springs were estimated using

$$K_{eq} = \frac{K_{1stshell} + K_{2ndshell}}{S_0}, \quad (2-14)$$

where S_0 is the number of springs to be inserted.

The values of equivalent spring constant K_{eq} obtained for all different CNTs are given in Table 5. Figure 14 shows that the van der Waals forces become more significant increasing diameter and increasing number of walls.

2E. Analysis procedure. The proposed SFS model was analyzed using the equivalent properties (EP) method for determining the CNTs properties. The equivalent properties method was defined based on the assumption that the deformation of two SFS-models could be equated when the applied load, CNT length, and area are equal. Here, the first SFS model was defined using a reference material and the second SFS was defined using the proposed orthotropic material. Based on the above definition, the CNT properties could be obtained from

$$\frac{E_{SFS-CNT}}{E_{SFS-Ref}} = \frac{\Delta L_{SFS-CNT}}{\Delta L_{SFS-Ref}}, \quad (2-15)$$

$$\frac{G_{SFS-CNT}}{G_{SFS-Ref}} = \frac{\Delta \theta_{SFS-CNT}}{\Delta \theta_{SFS-Ref}}. \quad (2-16)$$

The proposed analysis was carried out by constraining the CNT model at one end and applying a load at other end. As explained in the EP method, the C-C bond properties were assigned with a reference material and an orthotropic material individually. The first analysis was conducted with structured steel (reference material) properties of elastic modulus 200 GPa and a Poisson's ratio of 0.3. A similar analysis

zigzag (DWCNTs)

diameter (\AA)	first wall				second wall				K_{eq} (N/m)
	P_{end}	$P_{2\text{ndend}}$	total points	total working points	P_{end}	$P_{2\text{ndend}}$	total points	total working points	
5.481	16	16	168	124	30	30	384	302	1498
8.613	22	22	264	204	40	40	480	370	2017
10.962	28	28	336	259	46	40	552	442	2465
15.66	40	40	480	370	58	58	696	537	3189
21.924	60	60	672	507	74	74	936	733	4360

armchair (DWCNTs)

diameter (\AA)	first wall				second wall				K_{eq} (N/m)
	P_{end}	$P_{2\text{ndend}}$	total points	total working points	P_{end}	$P_{2\text{ndend}}$	total points	total working points	
5.424	16	16	161	117	36	36	359	260	1326
8.13	24	24	241	175	48	48	479	347	1836
0.84	32	32	321	233	52	52	519	376	2141
14.916	44	44	441	320	68	68	679	492	2855
21.696	64	64	641	465	84	84	839	608	3773

zigzag (MWCNTs)

diameter (\AA)	second wall				third wall				K_{eq} (N/m)
	P_{end}	$P_{2\text{ndend}}$	total points	total working points	P_{end}	$P_{2\text{ndend}}$	total points	total working points	
5.481	30	30	384	302	48	48	576	444	2623
8.613	40	40	480	370	58	58	696	537	3189
10.962	46	40	552	442	64	64	768	592	3579
15.66	58	58	696	537	76	76	912	703	4360
21.924	74	74	936	733	92	92	1104	851	5569

armchair (MWCNTs)

diameter (\AA)	second wall				third wall				K_{eq} (N/m)
	P_{end}	$P_{2\text{ndend}}$	total points	total working points	P_{end}	$P_{2\text{ndend}}$	total points	total working points	
5.424	36	36	359	260	56	56	560	406	2690
8.13	48	48	479	347	68	68	680	493	3418
10.84	52	52	519	376	72	72	720	522	3660
14.916	68	68	679	492	88	88	880	638	4630
21.696	84	84	839	608	104	104	1040	754	5601

Table 5. Equivalent spring stiffness values. For all cases, $K_{c-c} = 0.24245$ N/m.

zig zag (SWCNT)				
diameter (Å)	elastic modulus (GPa)		shear modulus (GPa)	
	pristine	vacancy defects	pristine	vacancy defects
5.481	768.525	260.328	320.259	104.663
8.61	769.163	245.471	322.764	89.1
10.96	769.231	235.844	323.164	87.5
15.657	770.442	220.186	320.189	83.5
21.92	774.39	209.463	311.66	70.3

armchair (SWCNT)				
diameter (Å)	elastic modulus (GPa)		shear modulus (GPa)	
	pristine	vacancy defects	pristine	vacancy defects
5.424	755.213	257.637	362.658	97.8
8.13	755.149	240.937	360.011	92.9
10.84	755.659	231.113	359.075	89.0
14.916	759.881	221.317	358.563	85.0
21.696	765.583	228.005	358.125	84.0

Table 6. Properties of pristine SWCNTs and SWCNTs with vacancy defects (zigzag and armchair).

was again carried out by using the orthotropic properties as explained in the previous section. Then the EP method was used to obtain the overall properties of the SFS CNT-model.

3. Results and discussion

The analysis was carried out for obtaining the elastic properties of single, double and multiwall CNTs configurations. The results clearly showed the effect of chirality, defects, number of walls, and the C-C bond orthotropic properties on the overall CNTs properties.

3A. Effect of chirality on the mechanical properties. Since the chirality defines the types of CNT configurations, both zigzag and armchair were modeled and analyzed. Table 6 shows the elastic and shear modulus values of both zigzag and armchair configurations of a single-wall carbon nanotube (SWCNT).

It is evident that the elastic modulus of the zigzag configuration is higher than the armchair one. The difference between the elastic modulus of the two configurations (zigzag and armchair) decreased as the CNT's diameter increased. On the other hand, the armchair configuration has a higher shear modulus than the zigzag. It is evident from these results that the chirality of the CNT primarily affected the shear strength rather than the tensile strength.

The variations in elastic and shear modulus for both zigzag and armchair configurations are attributed to the direction of the hexagonal unit cell to the applied tensile and torsional loads. For the zigzag configuration, all six C-C bonds of a hexagonal unit have contributed towards carrying the applied load (Figure 15a), while the armchair unit cell have used only four C-C bonds for the similar types of loading (Figure 15b). Therefore the tensile strength of zigzag is higher than armchair. However, for the torsional

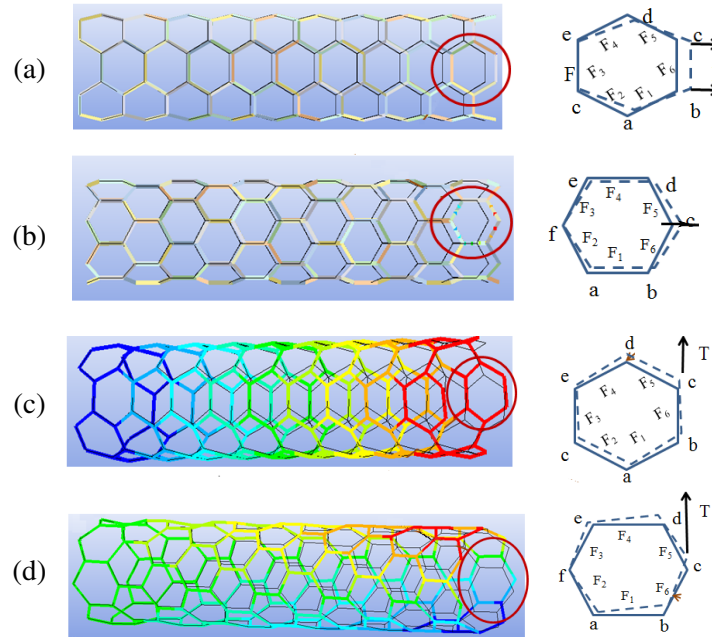


Figure 15. The deformation pattern of hexagonal units: armchair (a), zigzag-tensile load (b), armchair (c), and zigzag-applied moment (d).

loading, the reverse phenomenon could be seen as compared to the tensile loading (Figure 15c, d). The comparison based on chirality suggested that the zigzag SWCNTs of higher diameters could increase the properties of nanocomposites in the axial direction. For better transverse properties, armchair configurations with smaller diameters would be a better choice as a reinforcement.

The current analysis results align with the experimental values of 400 GPa to 800 GPa as given by Treacy [Treacy et al. 1996]. Further, the results are also comparable with the other numerical analysis carried out by Mohammad [Mohammadpour and Awang 2011], where they used the continuum mechanics method with nonlinear material properties and obtained the elastic properties of 881 GPa (elastic modulus) and 116 GPa (shear modulus). In addition, the molecular dynamics [Agrawal et al. 2006] results (elastic modulus 550–760 GPa for diameters in the range of 7–25 Å) for SWCNTs also align well with the SFS analysis results.

3B. Effect of vacancy defects. The elastic properties of both zigzag and armchair configurations of SWCNTs with vacancy defects were analyzed and their results were almost 70% lower than the corresponding pristine configurations (Table 6). In addition, the vacancy defects have shown more influence on both the elastic and shear modulus of both armchair and zigzag configurations as the diameter of the CNT was increased from 5.48 Å to 21.92 Å. The percentile decrease in CNT properties for the increase in diameter of a zigzag configuration was approximately 69.58% for the elastic modulus and 72.79% for the shear modulus. For the armchair configuration, the percentile decrease was 68.9% for the elastic modulus and 75.04% for the shear modulus, respectively (Table 7). Similar results were obtained by Ying

zigzag (SWCNT)		
diameter (Å)	elastic modulus (%)	shear modulus (%)
5.481	66.13	67.32
8.61	68.09	72.38
10.96	69.34	72.91
15.657	71.42	73.89
21.92	72.95	77.43
average	69.58	72.79

armchair (SWCNT)		
diameter (Å)	elastic modulus (%)	shear modulus (%)
5.424	65.89	73.01
8.13	68.09	74.19
10.84	69.42	75.19
14.916	70.87	76.29
21.696	70.22	76.53
average	68.9	75.04

Table 7. Percentile decrease of elastic and shear modulus due to vacancy defects (zigzag and armchair).

et al. [Yang et al. 2017] with elastic modulus of 270 GPa for SWCNTs with defects. Sakhaee [Sakhaee-Pour 2009] showed that the elastic and shear modulus of defective SWCNTs were 470 GPa and 160 GPa, respectively. The properties reported by these research works matched well with the results of the current research work.

It could be concluded from the results that the SWCNTs with armchair configuration with vacancy defects have shown better properties than the zigzag configuration. Moreover, the phenomenon was more significant for the diameter greater than 15 Å. From the above results, it could be pointed out that the armchair configuration with vacancy defects have shown improved properties compared to the zigzag configuration as the CNT's diameter increases.

3C. Effect of the number of walls. The effect of the number of walls on the CNTs properties were also analyzed using SFS CNT models. The elastic and shear modulus of both DWCNTs and MWCNTs approximately remains the same (Table 8). For the individual cases, the elastic modulus of the zigzag configuration is higher than armchair one and the armchair shear modulus is higher than the zigzag configuration. The elastic modulus varied inversely to the CNT's diameter until the value reached 15.697 Å and then the variation of elastic modulus became proportional to the CNT's diameter. The elastic modulus of DWCNT was higher at lower diameters and was gradually reduced as the CNT diameter reached 15.657 Å. Then, for further increases in diameter, the elastic modulus was increased again. For the MWCNT case, the elastic modulus values increased proportionally to the CNT's number of walls and the diameter. However, the shear modulus of both DWCNTs and MWCNTs increased as the diameter increased up to 15.697 Å, and then started to decrease with the increase in diameter.

zigzag				
diameter (Å)	elastic modulus DWCNT (GPa)	shear modulus DWCNT (GPa)	elastic modulus MWCNT (GPa)	shear modulus MWCNT (GPa)
5.481	794.199	320.235	794.199	320.23
8.61	783.311	322.752	783.311	322.75
10.96	770.318	323.312	770.318	323.31
15.657	761.661	328.514	761.661	328.51
21.92	782.353	311.379	782.353	311.38

armchair				
diameter (Å)	elastic modulus DWCNT (GPa)	shear modulus DWCNT (GPa)	elastic modulus MWCNT (GPa)	shear modulus MWCNT (GPa)
5.424	757.671	366.795	756.71	301.52
8.13	753.1	359.754	753.1	297.13
10.84	759.974	358.317	759.974	292.26
14.916	766.225	358.959	766.225	357.69
21.696	772.855	358.112	772.855	359.67

Table 8. Properties of DWCNTs and MWCNTs with zigzag and armchair CNTs.

type of CNT	diameter (Å)	elastic modulus (GPa)	shear modulus (GPa)	reference
DWCNT	10.0–30.0	1000–1100	400	[Li and Chou 2003a]
DWCNT zigzag	5.41–21.92	761–794	311–323	proposed SFS model
DWCNT armchair	5.424–21.69	753–772	358–366	
MWCNT	3.91–27.13	704	-	[Yu et al. 2000]
MWCNT	5–8	990–1029	213–228	[Sakhaee-Pour 2009]
MWCNT zigzag	5.41–21.92	761–794	310–323	proposed SFS model
MWCNT armchair	5.424–21.69	651–786	292–360	

Table 9. CNT elastic properties compared between the current study and other researches.

Table 9 shows a comparative analysis of results from other research works along with the current SFS model research work. It could be concluded here that the SFS structure with orthotropic C-C chemical bond could provide accurate elastic properties of both zigzag and armchair configurations for both pristine and CNTs with vacancy defects.

4. Conclusions and recommendations

In this research, the effect of chirality (zigzag and armchair), vacancy defects, and number of walls on the elastic properties of CNTs were characterized by the space frame structure method. The orthotropic properties of C-C bonds were calculated by comparing structural mechanics and molecular mechanics energy expressions along with a parametric study. A mathematical model using equivalent springs for van der Waals interactions between consecutive walls was developed to analyze their effect on DWCNTs and

MWCNTs. It has been found that the zigzag configuration elastic modulus was greater than the armchair configuration for CNTs with the same diameter. The shear modulus of the armchair configuration is greater than the zigzag configuration. Vacancy defects significantly reduced the elastic properties of SWCNTs and the effect of the vacancy defects increased as the diameter was increased further. The rate of decrease in the elastic and shear modulus of defective armchair nanotubes become insignificant as the diameter increased further. Comparatively DWCNTs have higher elastic modulus and shear modulus (average) than SWCNTs and MWCNTs for the smaller CNTs diameter range. The results shows that the SFS model elastic properties were in good agreement with the experimental and theoretical values found in the literature.

References

- [Agrawal et al. 2006] P. M. Agrawal, B. S. Sudalayandi, L. M. Raff, and R. Komanduri, "A comparison of different methods of Young's modulus determination for single-wall carbon nanotubes (SWCNT) using molecular dynamics (MD) simulations", *Comput. Mater. Sci.* **38**:2 (2006), 271–281.
- [Chabalala et al. 2011] V. P. Chabalala, N. Wagner, and S. Potgieter-Vermaak, "Investigation into the evolution of char structure using Raman spectroscopy in conjunction with coal petrography, I", *Fuel Process. Tech.* **92**:4 (2011), 750–756.
- [Ghavamian et al. 2013] A. Ghavamian, M. Rahmandoust, and A. Öchsner, "On the determination of the shear modulus of carbon nanotubes", *Compos. B Eng.* **44**:1 (2013), 52–59.
- [Han et al. 2014a] F. Han, Y. Azdoud, and G. Lubineau, "Computational modeling of elastic properties of carbon nanotube/polymer composites with interphase regions, I: Micro-structural characterization and geometric modeling", *Comp. Mater. Sci.* **81** (2014), 641–651.
- [Han et al. 2014b] F. Han, Y. Azdoud, and G. Lubineau, "Computational modeling of elastic properties of carbon nanotube/polymer composites with interphase regions, II: Mechanical modeling", *Comp. Mater. Sci.* **81** (2014), 652–661.
- [Harik 2011] V. Harik, *Mechanics of carbon nanotubes*, Nanodesigns Press, Newark, DE, 2011.
- [Hernández-Pérez and Avilés 2010] A. Hernández-Pérez and F. Avilés, "Modeling the influence of interphase on the elastic properties of carbon nanotube composites", *Comp. Mater. Sci.* **47**:4 (2010), 926–933.
- [Hu et al. 2007] N. Hu, K. Nunoya, D. Pan, T. Okabe, and H. Fukunaga, "Prediction of buckling characteristics of carbon nanotubes", *Int. J. Solids Struct.* **44**:20 (2007), 6535–6550.
- [Iijima 1991] S. Iijima, "Helical microtubules of graphitic carbon", *Nature* **354** (1991), 56–58.
- [Inam et al. 2014] F. Inam, A. Heaton, P. Brown, T. Peijs, and M. J. Reece, "Effects of dispersion surfactants on the properties of ceramic-carbon nanotube (CNT) nanocomposites", *Ceram. Int.* **40**:1 (2014), 511–516.
- [Jia et al. 2011] J. Jia, J. Zhao, G. Xu, J. Di, Z. Yong, Y. Tao, C. Fang, Z. Zhang, X. Zhang, L. Zheng, and Q. Li, "A comparison of the mechanical properties of fibers spun from different carbon nanotubes", *Carbon* **49**:4 (2011), 1333–1339.
- [Kundalwal and Kumar 2016] S. I. Kundalwal and S. Kumar, "Multiscale modeling of stress transfer in continuous microscale fiber reinforced composites with nano-engineered interphase", *Mech. Mater.* **102** (2016), 117–131.
- [Kundalwal and Ray 2014] S. I. Kundalwal and M. C. Ray, "Improved thermoelastic coefficients of a novel short fuzzy fiber-reinforced composite with wavy carbon nanotubes", *J. Mech. Mater. Struct.* **9**:1 (2014), 1–25.
- [Lennard-Jones 1924] J. E. Jones, "On the determination of molecular fields, I: From the variation of the viscosity of a gas with temperature", *Proc. R. Soc. Lond. A* **106**:738 (1924), 441–462.
- [Li and Chou 2003a] C. Li and T.-W. Chou, "Elastic moduli of multi-walled carbon nanotubes and the effect of van der Waals forces", *Compos. Sci. Technol.* **63**:11 (2003), 1517–1524.
- [Li and Chou 2003b] C. Li and T.-W. Chou, "A structural mechanics approach for the analysis of carbon nanotubes", *Int. J. Solids Struct.* **40**:10 (2003), 2487–2499.
- [Mohammadpour and Awang 2011] E. Mohammadpour and M. Awang, "Predicting a stretching behavior of carbon nanotubes using finite element method", pp. 374–378 in *Enabling science and nanotechnology* (Kuala Lumpur, 2010), edited by A. M. Hashim et al., AIP Conference Proc. **1341**, Amer. Inst. Physics, Melville, NY, 2011.

- [Muc 2010] A. Muc, “Design and identification methods of effective mechanical properties for carbon nanotubes”, *Mater. Des.* **31**:4 (2010), 1671–1675.
- [Muc 2011] A. Muc, “Modelling of carbon nanotubes behaviour with the use of a thin shell theory”, *J. Theor. Appl. Mech. (Warsaw)* **49**:2 (2011), 531–540.
- [Muthu and Dendere 2014] J. Muthu and C. Dendere, “Functionalized multiwall carbon nanotubes strengthened GRP hybrid composites: improved properties with optimum fiber content”, *Compos. B Eng.* **67** (2014), 84–94.
- [Nam et al. 2015] T. H. Nam, K. Goto, Y. Yamaguchi, E. V. A. Premalal, Y. Shimamura, Y. Inoue, K. Naito, and S. Ogihara, “Effects of CNT diameter on mechanical properties of aligned CNT sheets and composites”, *Compos. A Appl. Sci. Manuf.* **76** (2015), 289–298.
- [Popov et al. 2000] V. N. Popov, V. E. Van Doren, and M. Balkanski, “Elastic properties of single-walled carbon nanotubes”, *Phys. Rev. B* **61**:4 (2000), 3078–3084.
- [Qian et al. 2002] D. Qian, G. J. Wagner, W. K. Liu, M.-F. Yu, and R. S. Ruoff, “Mechanics of carbon nanotubes”, *Appl. Mech. Rev.* **55**:6 (2002), 495–533.
- [Rahmandoust and Öchsner 2009] M. Rahmandoust and A. Öchsner, “Influence of structural imperfections and doping on the mechanical properties of single-walled carbon nanotubes”, *J. Nano Res.* **6** (2009), 185–196.
- [Rahmandoust and Öchsner 2012] M. Rahmandoust and A. Öchsner, “On finite element modeling of single- and multi-walled carbon nanotubes”, *J. Nanosci. Nanotechnol.* **12**:10 (2012), 8129–8136.
- [Ranjbartoreh and Wang 2010] A. R. Ranjbartoreh and G. Wang, “Molecular dynamic investigation of mechanical properties of armchair and zigzag double-walled carbon nanotubes under various loading conditions”, *Phys. Lett. A* **374**:7 (2010), 969–974.
- [Reich et al. 2002] S. Reich, C. Thomsen, and P. Ordejón, “Elastic properties of carbon nanotubes under hydrostatic pressure”, *Phys. Rev. B* **65**:15 (2002), art. id. 153407.
- [Roy Chowdury et al. 2014] A. N. Roy Chowdury, C. M. Wang, and S. J. A. Koh, “Continuum shell model for buckling of armchair carbon nanotubes under compression or torsion”, *Int. J. Appl. Mech.* **6**:1 (2014), art. id. 145006.
- [Sakhaee-Pour 2009] A. Sakhaee-Pour, “Elastic properties of single-layered graphene sheet”, *Solid State Comm.* **149**:1-2 (2009), 91–95.
- [Sharma and Shukla 2014] K. Sharma and M. Shukla, “Three-phase carbon fiber amine functionalized carbon nanotubes epoxy composite: processing, characterisation, and multiscale modeling”, *J. Nanomater.* **2014** (2014), art. id. 837492.
- [Shokrieh et al. 2013] M. M. Shokrieh, A. Saeedi, and M. Chitsazzadeh, “Mechanical properties of multi-walled carbon nanotube/polyester nanocomposites”, *J. Nanostruct. Chem.* **3**:1 (2013), art. id. 20.
- [Tachibana 2013] M. Tachibana, “Characterization of laser-induced defects and modification in carbon nanotubes by Raman spectroscopy”, pp. 31–52 in *Physical and chemical properties of carbon nanotubes*, edited by S. Suzuki, IntechOpen, London, 2013.
- [Tersoff and Ruoff 1994] J. Tersoff and R. S. Ruoff, “Structural properties of a carbon-nanotube crystal”, *Phys. Rev. Lett.* **73**:5 (1994), 676–679.
- [Tjong 2013] S. C. Tjong, “Recent progress in the development and properties of novel metal matrix nanocomposites reinforced with carbon nanotubes and graphene nanosheets”, *Mater. Sci. Eng. R* **74**:10 (2013), 281–350.
- [Treacy et al. 1996] M. M. J. Treacy, T. W. Ebbesen, and J. M. Gibson, “Exceptionally high Young’s modulus observed for individual carbon nanotubes”, *Nature* **381** (1996), 678–680.
- [Tserpes et al. 2008] K. I. Tserpes, P. Papanikos, G. Labeas, and S. G. Pantelakis, “Multi-scale modeling of tensile behavior of carbon nanotube-reinforced composites”, *Theor. Appl. Fract. Mech.* **49**:1 (2008), 51–60.
- [Xiao and Hou 2006] S. Xiao and W. Hou, “Fracture of vacancy-defected carbon nanotubes and their embedded nanocomposites”, *Phys. Rev. B* **73**:11 (2006), art. id. 115406.
- [Yang et al. 2016] L. Yang, I. Greenfeld, and H. D. Wagner, “Toughness of carbon nanotubes conforms to classic fracture mechanics”, *Sci. Adv.* **2**:2 (2016), art. id. e1500969.
- [Yang et al. 2017] Y. Yang, C. Ramirez, X. Wang, Z. Guo, A. Tokranov, R. Zhao, I. Szlufarska, J. Lou, and B. W. Sheldon, “Impact of carbon nanotube defects on fracture mechanisms in ceramic nanocomposites”, *Carbon* **115** (2017), 402–408.

[Yu et al. 2000] M.-F. Yu, O. Lourie, M. J. Dyer, K. Moloni, T. F. Kelly, and R. S. Ruoff, “Strength and breaking mechanism of multiwalled carbon nanotubes under tensile load”, *Science* **287**:5453 (2000), 637–640.

[Zohdi and Wriggers 2005] T. I. Zohdi and P. Wriggers, *An introduction to computational micromechanics*, Lecture Notes in Appl. and Computational Mech. **20**, Springer, 2005.

[Zuberi and Esat 2015] M. J. S. Zuberi and V. Esat, “Investigating the mechanical properties of single walled carbon nanotube reinforced epoxy composite through finite element modelling”, *Compos. B Eng.* **71** (2015), 1–9.

Received 30 Nov 2017. Revised 8 Mar 2018. Accepted 28 May 2018.

MUHAMMAD ARIF: engrarifjan@gmail.com

School of Mechanical, Industrial and Aeronautical Engineering, University of the Witwatersrand, Johannesburg, South Africa

JACOB MUTHU: jacob.muthu@wits.ac.za

Department of Civil, Geological, and Environmental Engineering, University of Saskatchewan, Saskatoon, Canada

and

School of Mechanical, Industrial and Aeronautical Engineering, University of the Witwatersrand, Johannesburg, South Africa

JOURNAL OF MECHANICS OF MATERIALS AND STRUCTURES

msp.org/jomms

Founded by Charles R. Steele and Marie-Louise Steele

EDITORIAL BOARD

ADAIR R. AGUIAR	University of São Paulo at São Carlos, Brazil
KATIA BERTOLDI	Harvard University, USA
DAVIDE BIGONI	University of Trento, Italy
MAENGHYO CHO	Seoul National University, Korea
HUILING DUAN	Beijing University
YIBIN FU	Keele University, UK
IWONA JASIUK	University of Illinois at Urbana-Champaign, USA
DENNIS KOCHMANN	ETH Zurich
MITSUTOSHI KURODA	Yamagata University, Japan
CHEE W. LIM	City University of Hong Kong
ZISHUN LIU	Xi'an Jiaotong University, China
THOMAS J. PENCE	Michigan State University, USA
GIANNI ROYER-CARFAGNI	Università degli studi di Parma, Italy
DAVID STEIGMANN	University of California at Berkeley, USA
PAUL STEINMANN	Friedrich-Alexander-Universität Erlangen-Nürnberg, Germany
KENJIRO TERADA	Tohoku University, Japan

ADVISORY BOARD

J. P. CARTER	University of Sydney, Australia
D. H. HODGES	Georgia Institute of Technology, USA
J. HUTCHINSON	Harvard University, USA
D. PAMPLONA	Universidade Católica do Rio de Janeiro, Brazil
M. B. RUBIN	Technion, Haifa, Israel

PRODUCTION production@msp.org

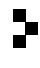
SILVIO LEVY Scientific Editor

See msp.org/jomms for submission guidelines.

JoMMS (ISSN 1559-3959) at Mathematical Sciences Publishers, 798 Evans Hall #6840, c/o University of California, Berkeley, CA 94720-3840, is published in 10 issues a year. The subscription price for 2018 is US \$615/year for the electronic version, and \$775/year (+\$60, if shipping outside the US) for print and electronic. Subscriptions, requests for back issues, and changes of address should be sent to MSP.

JoMMS peer-review and production is managed by EditFLOW[®] from Mathematical Sciences Publishers.

PUBLISHED BY

 **mathematical sciences publishers**
nonprofit scientific publishing

<http://msp.org/>

© 2018 Mathematical Sciences Publishers

Journal of Mechanics of Materials and Structures

Volume 13, No. 4

July 2018

- Prediction of springback and residual stress of a beam/plate subjected to three-point bending** **QUANG KHOA DANG, PEI-LUN CHANG, SHIH-KANG KUO and DUNG-AN WANG** **421**
- Characterization of CNT properties using space-frame structure** **MUHAMMAD ARIF and JACOB MUTHU** **443**
- Analytical approach to the problem of an auxetic layer under a spatially periodic load** **HENRYK KAMIŃSKI and PAWEŁ FRITZKOWSKI** **463**
- Stability and nonplanar postbuckling behavior of current-carrying microwires in a longitudinal magnetic field** **YUANZHUO HONG, LIN WANG and HU-LIANG DAI** **481**
- Three-dimensional Trefftz computational grains for the micromechanical modeling of heterogeneous media with coated spherical inclusions** **GUANNAN WANG, LEITING DONG, JUNBO WANG and SATYA N. ATLURI** **505**
- Uniform stress resultants inside two nonelliptical inhomogeneities in isotropic laminated plates** **XU WANG, LIANG CHEN and PETER SCHIAVONE** **531**
- An analytical solution for heat flux distribution of cylindrically orthotropic fiber reinforced composites with surface effect** **JUNHUA XIAO, YAOLING XU and FUCHENG ZHANG** **543**
- Strain gradient fracture of a mode III crack in an elastic layer on a substrate** **JINE LI and BAOLIN WANG** **555**
- Growth-induced instabilities of an elastic film on a viscoelastic substrate: analytical solution and computational approach via eigenvalue analysis** **IMAN VALIZADEH, PAUL STEINMANN and ALI JAVILI** **571**
- Application of the hybrid complex variable method to the analysis of a crack at a piezoelectric-metal interface** **VOLODYMYR GOVORUKHA and MARC KAMLAH** **587**



1559-3959(2018)13:4;1-Y